ELSEVIER

Analytica Chimica Acta 496 (2003) 117–131

ANALYTICA CHIMICA ACTA

www.elsevier.com/locate/aca

Surface vibrational sum frequency and Raman studies of PAMAM G0, G1 and acylated PAMAM G0 dendrimers

Anthony P. Davis [a], Gang Ma [b], Heather C. Allen [b,*]

[a] *US Coast Guard Academy (ds-1), New London, CT 06320, USA*

[b] *Department of Chemistry, The Ohio State University, 100 West 18th Avenue, Columbus, OH 43210, USA*

Received 17 May 2002; accepted 17 October 2002

Abstract

The first surface vibrational sum frequency generation (SFG) spectroscopic studies of amine-terminated Starburst® PAMAM G0 and G1 and acylated PAMAM G0 dendrimers at the glass–, gold–, and air–dendrimer interface are presented. Amine-terminated PAMAM G0 and G1 dendrimers as compared to the acylated PAMAM G0 dendrimer reveal significantly different surface SFG spectroscopic signatures. Raman spectra from PAMAM G0 and G1 dendrimers are presented for comparison of the bulk vibrational spectra to that of the surface. The SFG data is suggestive of skewed methylene conformations in a distribution about the normal of the surface.

Keywords: Surface vibrational sum frequency; SFG; BBSFG; Raman spectroscopy; PAMAM; Dendrimers

1. Introduction

Dendrimers are a unique class of polymers [1]. They are distinguished from randomly hyper-branched dendritic polymers in that each monomer joins the molecule at one site and adds two or more additional sites for further polymerization. The molecule expands with each successive generation of monomeric units in an extremely ordered, exponentially geometric fashion. When produced using a divergent synthesis, the polymers are constructed outwardly from a core molecule, such as ammonia or ethylenediamine. When produced using a convergent synthesis, the polymers are built from the periphery inward, joining fan-like branches called dendrons to a core molecule [1,2].

The potential for new dendrimer applications is as diverse as the very nature of the chemical versatility of dendrimers. They are well suited for new avenues in materials science as a distinctive classification of polymers, but due to their uniquely uniform structure, there are many other promising areas for which dendritic molecules are being developed. For example, as dendrimers grow generationally, they quickly become macromolecular in size. This allows one to remove larger dendrimers from a solution by simple filtration. Often, expensive catalysts are unrecoverable during the product work-up stage of a chemical reaction. A macromolecular dendrimer modified at the periphery with an appropriate catalyst could be recovered and recycled from a reaction mixture by filtration [3]. Another important application that shows promise is in the area of biomimicry. Many biologically significant molecules, including insulin, cytochrome C, and hemoglobin, are of the same

* Corresponding author. Fax: +1-614-292-1685.
E-mail address: allen@chemistry.ohio-state.edu (H.C. Allen).

0003-2670/$ – see front matter © 2003 Elsevier Science B.V. All rights reserved.
PII: S0003-2670(02)01375-2

spherical shape and diameter of certain dendrimer molecules [4]. Researchers have postulated that dendrimer molecules could be developed to carry out therapeutic functions by complexing the dendrimers with biologically relevant molecules. Dendrimers have already been used to mimic histone, a molecule used by the body to coil strands of DNA, for gene therapy research [3]. Another area of dendrimer research is that of drug delivery. Dendrimers of fourth or fifth generation tend to become rigid as the molecular periphery becomes highly populated and sterically crowded; likewise, the interior regions of these molecules are relatively hollow, providing protected space for a potentially sensitive molecule, e.g. a drug molecule. In this manner, a dendrimer could be developed to protectively carry a drug to a particular site in the body before it is released to carry out its function [5].

The creativity of the synthetic chemist has underscored the seemingly infinite ways in which dendritic molecules can be manipulated to express different properties and therefore potentially different functions. For example, researchers have shown that dendrimer generations can be functionally alternated, or radially layered. In one case, this was accomplished with hydrophilic amidoamine and hydrophobic organosilicon [6]. Another example of controlling the structure of dendrimers was shown by synthesizing dendrimers capable of intramolecular hydrogen bonding [7].

Among the physical properties of dendrimers that have garnished the most attention are molecular dimensions, uniformity of size and shape, degree of rigidity, location of terminating groups, and behavior on liquid and solid surfaces [8]. As the generation increases to generations two, three, and four, dendrimers begin to expand rapidly in size and mass. Further, while the molecular branches may still be relatively free in motion, the periphery of the molecule becomes more crowded until the molecule can no longer lie flat. Even in the least energetic conformation, the molecules are forced to take on a macromolecular, three-dimensional shape. Above generation four, dendrimers like PAMAM are considered to be globular and/or spherical in shape, and as the generations progress upward, the molecular periphery becomes more crowded until the molecules cannot accept the complete addition of another generation [8].

Various studies have begun to disclose other unique behaviors of dendrimers. For example, studies indicate that the size and dimensions of higher-generation PAMAM remain constant over changes of temperature and solvent quality, refuting the idea that these molecules can backfold to any substantial extent due to the change of environmental conditions [9]. On the other hand, PAMAM dendrimers have been shown to undergo pH-dependent internal conformational changes as the amines become protonated and carry a positive charge. The electrostatic repulsion between internal amines may drive the dendrimer into a more expanded configuration, encouraging the branches to spread out [10]. There is a body of literature discussing energy transport within dendrimers [11] and fluorescence studies [12,13]. There are a relatively few publications discussing the infrared spectra of PAMAM dendrimers [14–17] and even fewer publications discussing Raman spectroscopic studies of dendrimers in general [18].

Although there has been a significant amount of research completed to date, there still remain many questions as to the structural conformation of dendrimers, each having their own individual properties. PAMAM dendrimers, perhaps because of their commercial availability, have been studied and modified extensively by researchers probing the unique nature of these macromolecules. However, there are currently no published accounts using surface vibrational sum frequency generation spectroscopy to study dendrimers at surfaces.

It is important to understand molecules such as PAMAM dendrimers at interfaces due to their potential applications. With the many exciting prospects ahead for the future of dendritic polymers, understanding the intramolecular and intermolecular structure/orientation of dendrimers and how this orientation is affected by the chemical and physical environment, i.e. at various interfaces, are important since structure and function are related. This inevitably requires the utilization of analytical techniques well suited to investigate these properties.

Molecular behavior at surfaces and interfaces can be quite unique. Changes in interfacial behavior can potentially influence practical applications in that surface activity can alter molecular uptake by a surrounding environment, or perhaps a tendency toward

monolayer self-assembly could lead to coating, film, and/or membrane applications.

Studying surfaces and interfaces ushers in completely different challenges, as there are few analytical techniques that can differentiate between a surface or interface and the bulk properties of a substance. A surface-specific optical technique that has been gaining prominence in the past 15 years is surface vibrational sum frequency generation (SFG) spectroscopy. Second order nonlinear techniques such as sum frequency (SF) spectroscopy depend upon lack of inversion symmetry at the microscopic and macroscopic scale for signal intensity. While centrosymmetric media possess symmetry about a center of inversion, all substances are asymmetrical at a surface, more appropriately referred to as an air–liquid, air–solid, liquid–liquid, liquid–solid, or solid–solid interface.

Other surface technologies have been utilized to study dendrimers at surfaces. Atomic force microscopy has been used extensively to study molecular dimensions, shape, and orientation of dendrimers on surfaces [19–24]. A plethora of other studies exist probing various surface dendrimer properties, such as measuring adsorption with a quartz crystal microbalance [25], testing chemical sensor potential with a surface acoustic wave mass balance [14], observing dendrimer adsorption onto a self-assembled monolayer by attenuated total reflectance surface enhanced infrared absorption spectroscopy [15], and another study that combined some of these techniques with ellipsometry, contact-angle measurements, ac-impedance spectroscopy, and cyclic voltammetry to observe the orientation of PAMAM dendrimers on different types of surfaces [26]. A recent review by Tully and Fréchet [27] concluded that dendrimers are well suited for application at interfaces since the unique dendritic structure gives rise to unusual chemical and physical properties. Thus, any new analytical technique that can help to better explain the behavior of these unique molecules at interfaces would be of considerable benefit.

A reasonable approach for studying SFG and Raman spectra of dendrimers would be to modify the PAMAM dendrimer in such a way as to alter their vibrational spectra in the CH stretching region to simplify interpretation. Infrared frequencies currently employed in SFG spectroscopic methods are generally in the 2000–3800 cm^{-1} region due to the difficulties associated with producing high mode-quality short IR laser pulses. One method is to append a deuterated methyl functionality to the periphery of the PAMAM molecules, so that the methyl CH stretching frequencies would be red-shifted away from the large aliphatic CH stretch absorption. Considering the size of PAMAM dendrimer molecules and the abundance of methylene groups, their vibrational spectra will have no shortage of vibrational modes in the aliphatic CH stretch region. Even PAMAM G0, the smallest PAMAM dendrimer, has 246 modes and 18 methylene groups. Thus, the difficulty arises in spectral interpretation, and, therefore, deuteration of the PAMAM terminating groups would help facilitate spectral assignment.

In this paper, we present data on the CH vibrational character of the first two generations of the Starburst® PAMAM (poly(amidoamine)) dendrimer, G0 and G1. Although we are currently synthesizing the acylated PAMAM G0 and G1 with end groups terminating in CD_3 for further vibrational characterization, this is beyond the scope of this paper. Here, vibrational data is presented from the bulk condensed phase using Raman spectroscopy and at the air–, glass–, and gold–dendrimer interfaces using broadband sum frequency generation (BBSFG) spectroscopy. In addition, BBSFG of an acylated PAMAM G0 dendrimer (–NH_2 converted to –$NH(CO)CH_3$) are presented.

1.1. Sum frequency generation theory

Sum frequency generation has been utilized for investigations of surfaces for more than a decade. The theory has been described previously [28–31]. However, a brief overview of the theory is presented here. SFG is a second order nonlinear optical process. Under the electric-dipole approximation, SFG is forbidden in media with inversion symmetry but allowed at surfaces and interfaces where inversion symmetry is broken. Therefore, SFG can be used as a surface-selective analytical probe. The SFG intensity I_{SFG}, as shown in Eq. (1), is proportional to the absolute square of the macroscopic second order nonlinear susceptibility, $\chi^{(2)}$, which consists of a resonant term $\chi_R^{(2)}$ and a nonresonant term $\chi_{NR}^{(2)}$.

$$I_{SFG} \propto |\chi^{(2)}|^2 \propto \left| \chi_{NR}^{(2)} + \sum_{\nu} \chi_{R_\nu}^{(2)} \right|^2 \quad (1)$$

When the frequency of an incident infrared beam, ω_{IR}, is resonant with a surface vibrational mode ν that is both infrared and Raman active, the resonant susceptibility term dominates the intensity of the SFG response. The resonant macroscopic nonlinear susceptibility, $\chi^{(2)}_{R_\nu}$, is shown in Eq. (2),

$$\chi^{(2)}_{R_\nu} \propto \frac{A_\nu}{\omega_\nu - \omega_{IR} - i\Gamma_\nu} \quad (2)$$

where A_ν is the strength of the transition moment, ω_ν is the frequency of the transition and Γ_ν is the line-width of the transition. The amplitude, A_ν, is nonzero when the Raman and the infrared transitions are spectroscopically allowed. $\chi^{(2)}_{R_\nu}$ is related to the molecular hyperpolarizability, β_ν, shown in Eq. (3), by the number density of surface species, N, and an orientationally averaged Euler angle transformation, $\langle \mu_{IJK:lmn} \rangle$, between the laboratory-coordinate (I, J, K) and the molecule-coordinate (l, m, n).

$$\chi^{(2)}_{IJK,R_\nu} = N \sum_{lmn} \langle \mu_{IJK:lmn} \rangle \beta_{lmn,R_\nu} \quad (3)$$

The surface susceptibility $\chi^{(2)}$ is a 27-element tensor and can be reduced by invoking symmetry constraints. If an azimuthally isotropic interface is assumed, only four independent components of $\chi^{(2)}$ are nonvanishing. These are χ_{zzz}, $\chi_{xxz} = \chi_{yyz}$, $\chi_{zxx} = \chi_{zyy}$, $\chi_{xzx} = \chi_{yzy}$, where z is chosen to be along the surface normal and x in the incident plane. The four $\chi^{(2)}$ components can be deduced by collecting the SFG response using different polarization combination measurements, SSP (S: S-polarized sum frequency; S: S-polarized 800 nm; P: P-polarized infrared), SPS, PSS, PPP. The different polarization combinations are sensitive to different $\chi^{(2)}$ components. In this study, the SSP polarization combination was utilized.

The theory of broadband sum frequency generation (BBSFG) is the same as that for sum frequency. Typically in sum frequency generation spectroscopy, the infrared frequencies are narrowband and must be scanned. The SFG response is then obtained one data point at a time. Broadband sum frequency generation utilizes a broad bandwidth infrared beam and a narrow bandwidth 800 nm beam. The broad bandwidth IR beam allows for probing a large spectral region without scanning the infrared frequency. This allows the full SFG spectrum to be acquired from one pulse.

2. Experimental

2.1. Instrumentation

Proton NMR spectra were obtained with a Bruker DPX-400 NMR spectrometer using a 30° tip angle, a 1 s recycle time, and 16 scans. The ^{1}H NMR spectra were calibrated to the d_4-methanol quintet at 3.31 ppm [32].

The Raman experimental setup consisted of a 785 nm CW laser (Process Instruments Inc.), a 5 mm focusing Raman Probe (InPhotonics Inc.), a 500 mm monochromator (Acton Research SpectraPro SP-500) using an 1800 g/mm holographic grating and a back-illuminated charge-coupled device camera (1340 × 400 pixel array; Roper Scientific LN400EB-deep depletion CCD). The illumination fiber optic of the Raman probe allowed for illuminating the dendrimer sample and the Raman backscatter was collected through the second (collection) fiber optic after passing through the detection optics. The collection fiber was connected to the entrance slit of the monochromator. SpectraSense software (Acton Research version 4.0.6) was used for data collection and display. For the Raman measurements, the sample was contained in a glass vial and placed in a home-built Raman collection stage that also housed the Raman probe. Power measurements at the end of the probe indicated that the sample was subjected to ~75 mW of CW 785 nm laser light. (Initially, 532 nm CW light was utilized; however, the fluorescent background of the samples of PAMAM G0 and G1 interfered with the measurement.) Raman spectral resolution was 5 cm^{-1}.

Details of the setup for the broadband sum frequency generation spectroscopy experiment have been described previously [33]. However, the system has been modified slightly, and therefore a brief description will be given here. The BBSFG system consists of two regenerative amplifiers (Spectra-Physics Spitfire, fs and ps versions), both of which are seeded by a sub-50 fs 800 nm pulse from a Ti: Sapphire oscillator (Spectra-Physics Tsunami). The oscillator is pumped by 4.7 W from a Nd:YVO_4 CW laser (Spectra-Physics Millennia Vs). The regenerative amplifiers are pumped by an all solid-state Nd:YLF laser (Spectra-Physics Evolution 30, 527 nm); 8 and 12 W are used in the fs and ps regenerative amplifiers, respectively. The all

solid-state Nd:YLF replaced the flash lamp-pumped Nd:YLF that was used previously. This system modification has substantially improved the hour-to-hour stability of the system. The output of the 1 kHz repetition rate regenerative amplifiers provides 85 fs pulses at 800 nm (22 nm bandwidth) and 2 ps pulses at 800 nm (17 cm^{-1} bandwidth). The fs broad bandwidth pulses are then used to generate broad bandwidth infrared (~600 cm^{-1} bandwidth) light via an optical parametric amplifier (Spectra-Physics OPA-800CF). The SFG experiment was performed in reflection geometry using the narrow bandwidth ps 800 nm beam and the broadband infrared beam. The two input beams, fs and ps, are overlapped at the sample surface spatially and temporally to produce a vibrationally-resonant sum frequency generation spectrum. The infrared and 800 nm beams were incident on the sample at 66° and 58° from the surface normal, respectively. The SFG photons were emitted at 59.3° from the surface normal and were detected using a 500 mm monochromator-CCD system (Acton Research SpectraPro SP-500; 1340 × 400 pixel array, Roper Scientific LN400EB back-illuminated CCD) with a 1200 g/mm grating blazed at 750 nm. The narrow bandwidth ps pulses limit the BBSFG spectral resolution. The polarization combination for the studies presented here were SSP (S: SFG, S: 800 nm, P: infrared). The input energies of the 800 nm and infrared beams were 50 and 10 μJ, respectively. The nonresonant SFG spectrum of a GaAs crystal surface was obtained both with and without a polystyrene film covering the OPA output port. The resulting SFG spectra were used for normalization purposes and as a reference to calibrate the peak positions of the BBSFG spectra.

2.2. Chemicals and materials

Starburst® PAMAM generations 0 and 1 dendrimers (20 wt.% methanol solutions) were purchased from Aldrich and used without further purification. Sodium dodecyl sulfate (purity > 99%) was purchased from Fisher Scientific and used without further purification. Nanopure water of 18 MΩ resistivity was used.

Glass slides were purchased from Fisher Scientific and were cleaned with an oxidizing agent in sulfuric acid, thoroughly rinsed with Nanopure water, and then dried in an oven (>70 °C) for several hours before use in the SFG experiments. Dendrimer deposition was performed by placing one drop (0.02 ml) of the 20 wt.% PAMAM G0 and G1 in methanol onto a glass slide, and 1 h was allowed for methanol evaporation. For dendrimer deposition of the modified PAMAM dendrimer, one drop (0.02 ml) of 1.4 wt.% acylated PAMAM G0 in methanol was deposited onto a glass slide, and 1 h was allowed for methanol evaporation. The surface coverage of the PAMAM G0, G1, and acylated G0 dendrimers were calculated to be 9×10^{17} cm^{-2}, 2×10^{17} cm^{-2}, and 2×10^{16} cm^{-2}, respectively. Clearly, multiple layers of dendrimer were deposited on the glass surface.

The bare gold surface film was purchased from Edmund Scientific and cleaned with spectrophotometric grade methanol prior to PAMAM dendrimer deposition. One drop (0.02 ml) of the PAMAM G0 dendrimer 5 wt.% in methanol solution was deposited on the gold surface and the methanol was allowed to evaporate. After 1 h, the BBSFG spectrum was recorded. The multilayer surface coverage was estimated to be 2×10^{17} cm^{-2}.

2.3. PAMAM acylation synthesis and NMR analysis

The acylated PAMAM G0 was synthesized by reacting PAMAM G0 with acetic anhydride using 4-dimethylaminopyridine (DMAP) as a hypernucleophilic catalyst. The methanol was removed from the dendrimer reagent by rotary evaporation. The resultant pure dendrimer was then dried under high vacuum in an acetone-reflux drying pistol overnight. Then, the gel-like dendrimer was dissolved in dimethylformamide (DMF). Excess (40 equivalents) poly(4-vinylpyridine) powder and 1/20 of an equivalent of DMAP were added into the dendrimer/DMF solution. Forty equivalents of acetic anhydride (10 × excess) were slowly added into the dendrimer/DMF solution drop-wise, and the reaction was left stirring for 6 days. The residual solids in the solution were removed by vacuum filtration and then by centrifuge. The DMF was removed from the product solution by high vacuum evaporation under heat (50 °C) into a Kugelrohr bulb to isolate the crude product. The crude product was dissolved in a minimal amount of methanol, and then the methanol solution was transferred into toluene. The precipitated dendrimer product was vacuum-filtered from the toluene and dried in an oven.

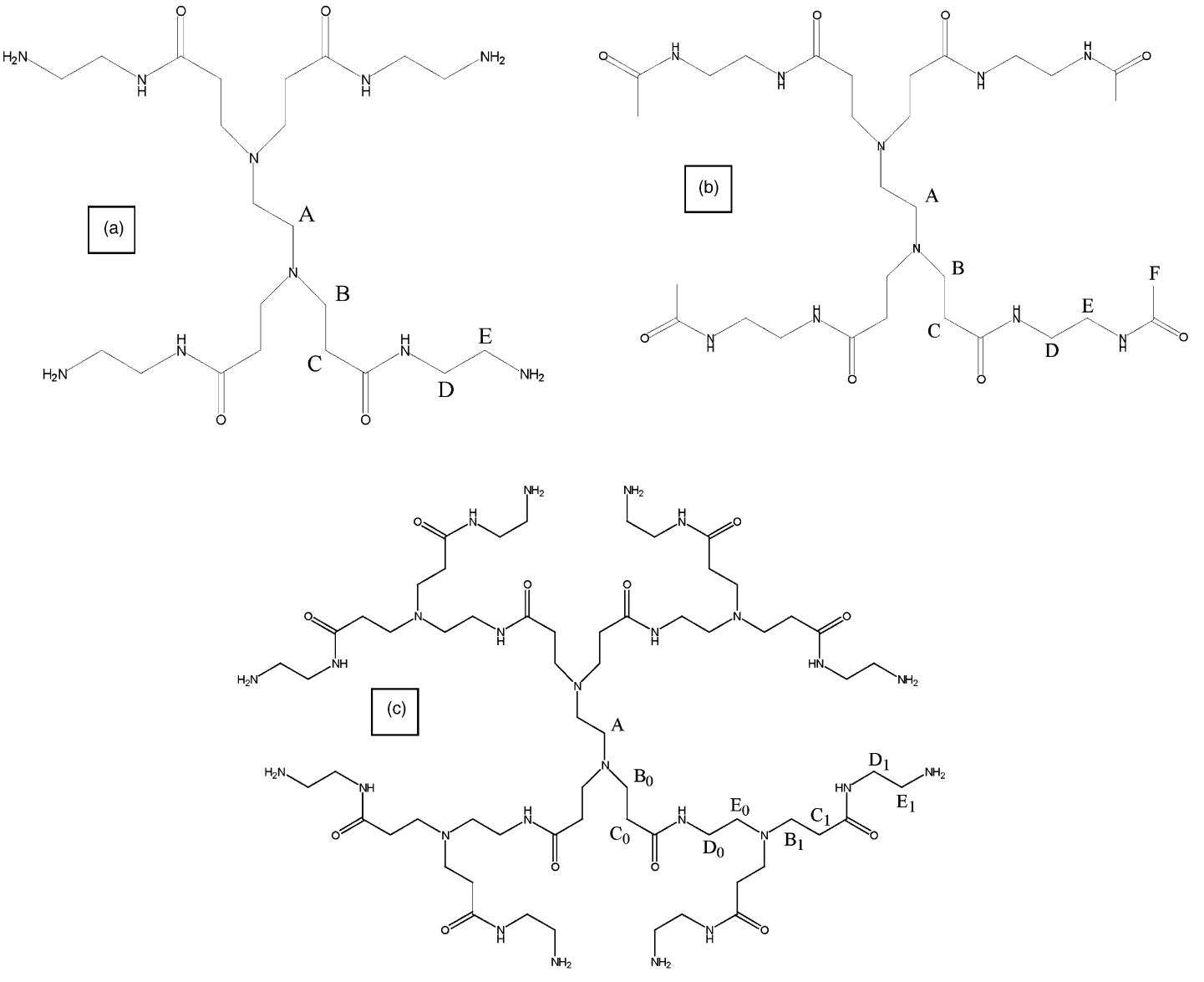

Fig. 1. (a) Schematic of PAMAM G0; (b) Acylated PAMAM G0; and (c) PAMAM G1.

PAMAM dendrimers become structurally complex with each additional generation, and therefore, schematics of the PAMAM dendrimers used in this study are shown in Fig. 1a–c. Amine-terminated PAMAM G0 and the synthetically modified PAMAM G0 are shown in Fig. 1a and b. As illustrated in Fig. 1b, the PAMAM G0 was acylated, thereby adding a—$(CO)CH_3$ as the terminating group of the dendritic arms. In Fig. 1c, amine-terminated PAMAM G1 is shown schematically. Although we have also acylated this molecule, studies presented here focus on the acylated G0 product and the nonmodified PAMAM G0 and G1 dendrimers.

Before the vibrational spectroscopic studies were conducted, the purities of the purchased PAMAM reagents and of the acylated PAMAM were analyzed using ^{1}H NMR. In order to assign the chemical shifts observed from the AcPAMAM NMR spectrum, and because NMR was used to identify the AcPAMAM product, it was necessary to first examine the ^{1}H NMR spectra from the starting material PAMAM dendrimers, G0 and G1.

In Fig. 1 a–c, the letters adjacent to the chemical groups are shown for NMR referencing purposes, since each group of hydrogen atoms can be differentiated according to their local chemical environment. Shown in Fig. 2a is the proton NMR spectrum from PAMAM G0 (refer to the schematic in Fig. 1a). The two sets of protons centered at the ethylenediamine core (carbon A) are only capable of coupling with each other; therefore, they are represented as a singlet, rather than a triplet, observed at 2.54 ppm. The next two sets of protons, on carbons B and C, couple with each other, and so they are each represented as triplets bearing coupling constants near 6.8 Hz. Matching these peaks to empirical predictions indicated that the carbon B protons are centered at 2.77 ppm, while the carbon C protons are centered at 2.36 ppm. Carbon atoms D and E are very similar to carbon atoms B and C in that they are represented by triplets centered at 3.25 and 2.72 ppm, respectively. In the inset of Fig. 2a, the ^{1}H NMR spectrum from the acylated PAMAM G0 (AcPAMAM) dendrimer is shown. AcPAMAM G0 has seven chemically unique sets of protons, labeled as A–F in Fig. 1b. As similar as this molecule is to the nonacylated PAMAM G0, so are the NMR spectra of AcPAMAM G0 and PAMAM G0. The change between PAMAM G0 and AcPAMAM G0 causes only two structurally significant differences: 1) the addition of a methyl functionality, giving rise to a singlet near 2.0 ppm, and 2) carbon E changes from a primary amine to an amide, causing the D and E triplets to merge into a singlet near 3.3 ppm. It can be shown that the protons on carbon atoms D and E have become chemically equivalent by tracing the molecule as far as four bonds from each proton; NMR deshielding effects are generally only significant as far as two bonds from a particular atom. The spectrum was unchanged with respect to protons A–C.

Shown in Fig. 2b is the ^{1}H NMR spectrum from the PAMAM G1 dendrimer. Similar to the PAMAM G0 molecule, chemical equivalence can be observed in the G1 molecule amongst all atoms found equidistant from the center of the core. Counting from the center, PAMAM G1 has nine chemically unique sets of protons, labeled A, $B_0 - E_0$, and $B_1 - E_1$ in Fig. 1c. The subscript numbers 0 and 1 denote the generation to which a carbon atom belongs; there is a noticeable structural similarity amongst carbon atoms labeled with the same letter in each generation. All of these carbon atoms are covalently bonded to two chemically equivalent hydrogen atoms, with the exception of carbon atoms D_0 and D_1, the amide carbonyls.

Due to the structural similarities between PAMAM G0 and G1, one can predict that the ^{1}H NMR spectrum will be essentially the same as that of PAMAM G0, with one notable exception: Carbon atom E_0, bonded to a primary amine in generation 0, is now bonded to a tertiary amine, while their counterparts at E_1 are still a primary amine. In this respect, the carbon E_0 protons are more similar to the core protons, and the E_1 protons are more similar to the E protons of generation 0. The carbon A protons are represented as a singlet in Fig. 2b observed at 2.58 ppm, and they are superimposed by a triplet at 2.59 ppm, representing the E_0 protons coupling with D_0. Carbon atoms, B_{0-1}, C_{0-1}, and D_{0-1} are all represented as overlaying triplets in the same relative positions as the corresponding chemical shifts in the spectrum of generation 0. Although the triplets for each corresponding set of methylene protons overlap, they are not indistinguishable. The generation 1 triplets are slightly offset from generation 0 and are significantly larger due to having twice as many protons per molecule as the lower generation PAMAM G0. The ^{1}H NMR spectra shown in Fig. 2a and b demonstrate the purity

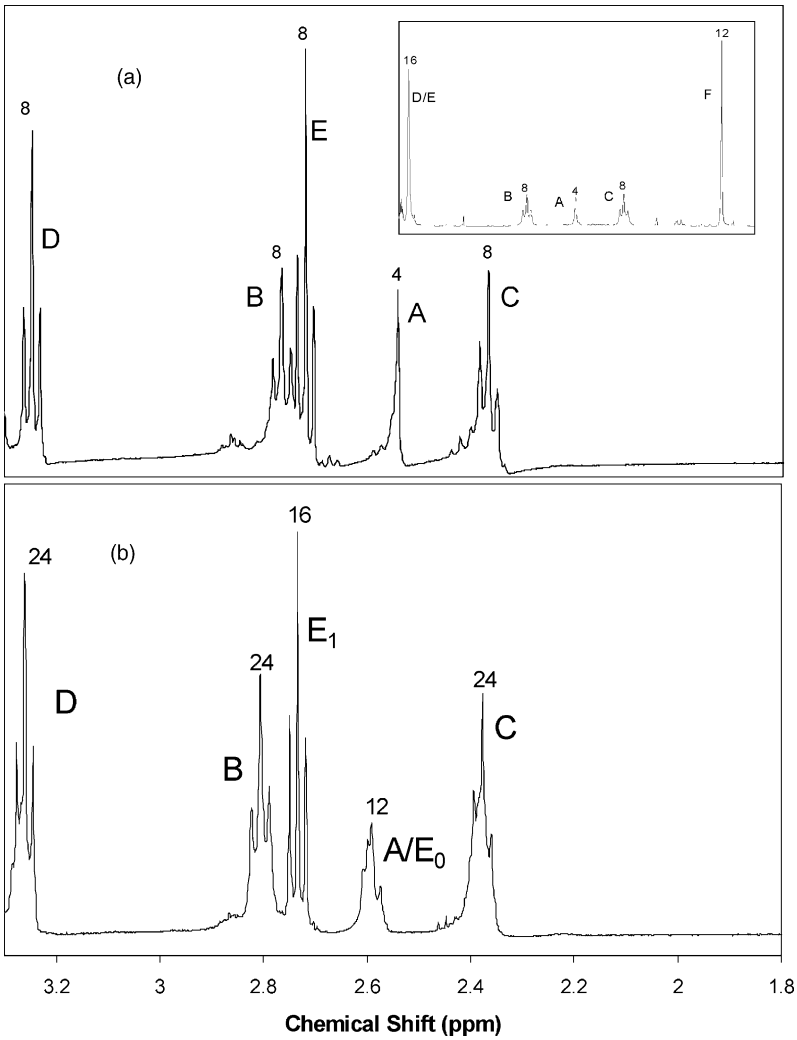

Fig. 2. (a) Proton NMR of PAMAM G0. Inset: Ac-G0; (b) Proton NMR of PAMAM G1. Letters correspond to the type of hydrogen and are to be compared with the corresponding letters in Fig. 1a–c. Numbers are integrated values.

of the PAMAM dendrimers used for the vibrational studies.

3. Results and discussion

Understanding the Raman spectra from the PAMAM dendrimers in the CH stretching region is important to the surface spectroscopy studies since SFG depends upon Raman transition moments in addition to infrared transition moments. There are relatively few published accounts of infrared vibrational spectroscopy for PAMAM dendrimers in the literature that provide substantial details on the spectral assignments [16,17], and to our knowledge, there are no Raman spectra published to date of PAMAM dendrimers [16,34]. For the Raman studies, the methanol solvent was evaporated from the 20 wt.% dendrimer–methanol solution to produce a pure dendrimer gel. The Raman spectrum of PAMAM G0 in Fig. 3 shows the spectral region from 2500 to 3200 cm^{-1}, which is in the CH stretching region. Although Raman and infrared

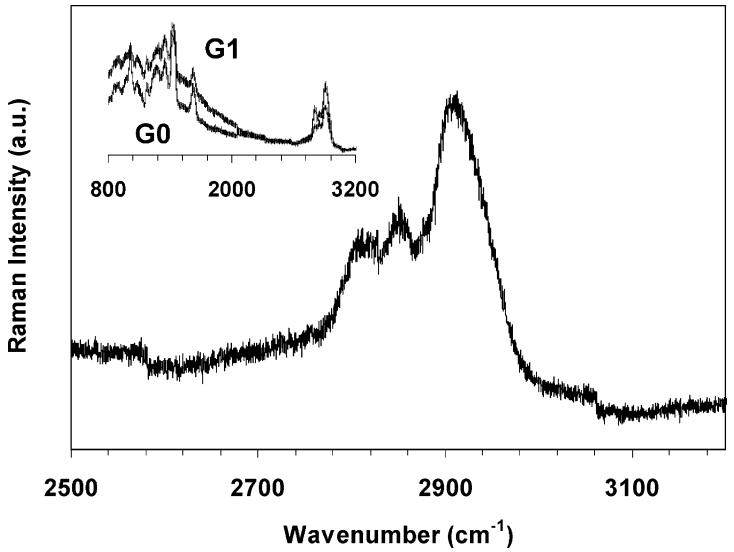

Fig. 3. Raman spectrum showing the CH stretching region of the amine-terminated PAMAM G0 dendrimer. Inset: Raman spectrum from 800 to 3200 cm^{-1} (excitation source: 785 nm CW laser, 75 mW).

frequencies do not exactly correspond with one another, these frequencies are generally within a few wavenumbers, and therefore, previously published infrared frequencies were used as a reference for our peak assignments. In Fig. 3, the peaks observed at 2820 cm^{-1} and at 2855 cm^{-1} are assigned to the CH_2 symmetric stretching (SS) modes with additional contribution from CH_2 Fermi resonance (FR) modes on the higher energy side of the CH_2-SS peaks. The peak observed at 2910 cm^{-1} is assigned to CH_2 asymmetric stretching (AS) modes. According to previously published infrared (FTIR) assignments [16], 2830 and 2907 cm^{-1} (additionally 2868 and 2943 cm^{-1}) are attributed to the CH_2-SS and the CH_2-AS modes, respectively. Our assignments are consistent with the previously published infrared frequencies, although a thorough experimental and theoretical study would greatly improve the understanding of the vibrational character of the CH stretching region from PAMAM dendrimers. It is not clear that all of the CH_2 symmetric stretches and asymmetric stretches from PAMAM G0 and G1 would lie cleanly within each observed band. Preliminary calculations of the vibrational frequencies in our laboratory have indicated that this may not be the case.

In the inset of Fig. 3, the Raman spectra of both PAMAM G0 and G1 in the region of 800–3200 cm^{-1} are shown. Peak assignments for the spectral region below 2500 cm^{-1} are beyond the scope of this paper; however, as one might expect, the Raman spectra of the PAMAM G0 and G1 are clearly similar and reflect intensity changes that are consistent with the structural differences between PAMAM G0 and G1 dendrimers. The amine/amide peaks, although observed in IR spectra [16] at 3068 and 3272 cm^{-1} are not of enough intensity to decipher in our Raman spectra in Fig. 3, nor in the inset, due in part to lower detection efficiencies in the near IR (>3000 cm^{-1} frequencies correspond to detection of $\lambda > 1027$ nm for 785 nm excitation).

A fluorescence background is clearly observed in the spectral region below 2000 cm^{-1} of PAMAM G0 and G1 shown in the inset of Fig. 3. The Raman spectra were obtained using a 785 nm CW laser since prior attempts using a 532 nm CW laser proved too difficult to decipher due to the large fluorescence background. The fluorescence is observed as a broad background in the Raman spectra and is consistent with an $n \rightarrow \pi^*$ transition from the amido groups throughout the PAMAM structure, which has been observed and discussed by Larson and Tucker [12]. The fluorescence observed from the AcPAMAM G0 dendrimer when using the 785 nm excitation laser light made the acquisition of the AcPAMAM G0 Raman spectrum non-

decipherable since the fluorescence background overwhelmed the scattering intensity from the vibrational modes, similar to the problem experienced when using the 532 nm laser for the PAMAM G0 and G1 dendrimers. In the Raman spectra shown in Fig. 3 and in the inset of Fig. 3, CCD detection efficiency limits the ability to observe weak Raman intensities beyond 3000 cm^{-1}.

Fig. 4a and b show the surface vibrational BBSFG spectra of PAMAM G0 and G1 dendrimers obtained after deposition of the dendrimer on the glass slide. The methanol was allowed to evaporate off for 1 h, and

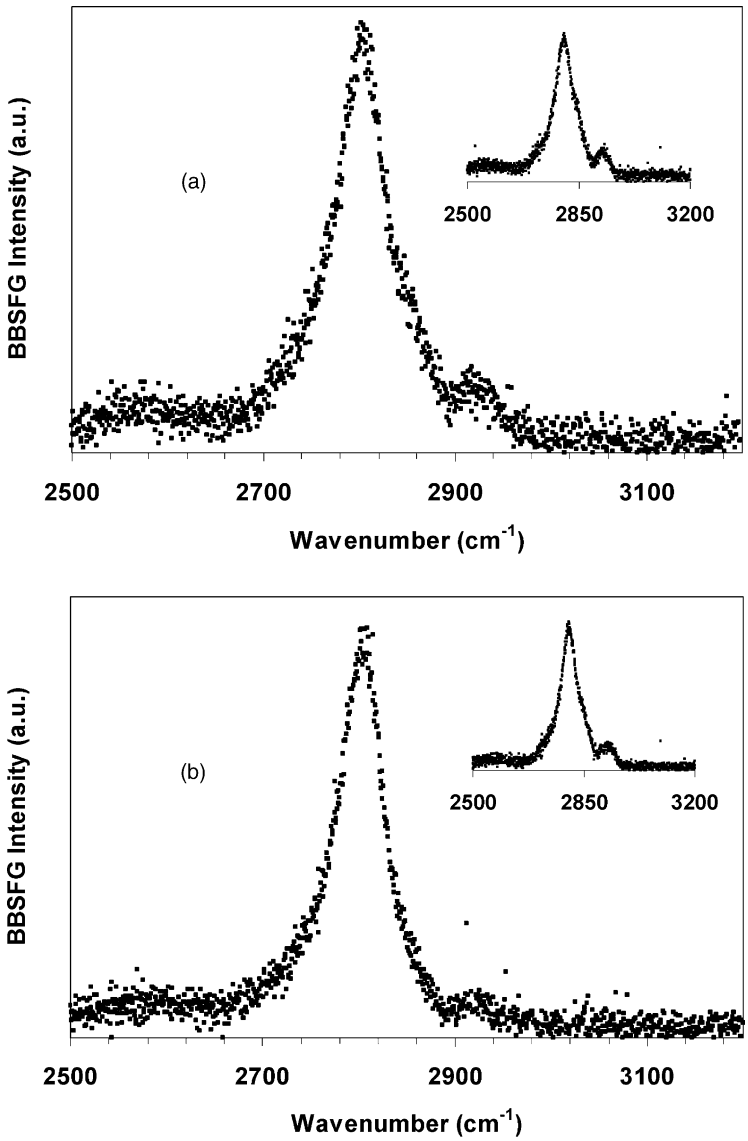

Fig. 4. (a) BBSFG spectrum (SSP polarization) of PAMAM G0 after deposition on a glass slide using a 5 min acquisition time. Inset: 36 h after deposition (5 min acquisition time); (b) BBSFG spectrum (SSP polarization) of PAMAM G1 after deposition on a glass slide using a 5 min acquisition time. Inset: 36 h after deposition (5 min acquisition time).

then the spectra were obtained. The inset of Fig. 4a and b show the BBSFG spectra from the same samples, G0 and G1, respectively, obtained 36 h after the initial methanol evaporation. In the four spectra shown in Fig. 4a and b, and their insets, two SF peaks are observed at 2802 and 2920 cm^{-1}. Based on the Raman assignments discussed above, the peak at 2802 cm^{-1} is assigned to CH_2-SS modes, and the peak at 2920 cm^{-1} is assigned to CH_2-AS modes, although there may also be an irresolvable contribution from the CH_2-FR on the high-energy side of the 2802 cm^{-1} band.

The ratio of the relative intensity of the CH_2-AS peak (2920 cm^{-1}) versus the CH_2-SS peak (2802 cm^{-1}) and the sharpening of the CH_2-AS peak in the insets of Fig. 4a and b reveal that the CH_2 groups on the dendron arms of the PAMAM G0 and G1 dendrimers have slightly changed in their relative surface conformation over the 36 h period. The ratio of the relative intensity of these two peaks (AS:SS) within each spectrum has increased from 0.14 to 0.22 for the PAMAM G0 (Fig. 4a and inset) and from 0.08 to 0.17 for the PAMAM G1 (Fig. 4b and inset). A likely explanation is that the dendrimers had not reached their stable conformation at the time that the initial spectra were recorded. After 36 h, the SFG spectra reveal a larger and slightly narrower CH_2-AS peak, which infers that there is a concerted orientation of the dendron arms of the dendrimer. Using the SSP polarization combination, if the CH_2 groups are situated relatively normal to the surface plane, a large symmetric stretch relative to the size of the asymmetric stretch would be observed. This is what we observe from Fig. 4a and b. However, after 36 h, the AS has changed inferring a more ordered but less upright configuration of the CH_2 groups.

We have further investigated the structural implications of these measurements by comparing the spectrum in Fig. 4a with a BBSFG spectrum taken of a monolayer of sodium dodecyl sulfate (SDS) formed from a 1 mM SDS solution. Shown in Fig. 5 are the spectra from the surface of the SDS solution and from the surface of the PAMAM G0 dendrimer gel. Both spectra were recorded under exactly the same conditions using a 2 min acquisition time for both. SDS has been studied extensively using SFG [29,30] and it is therefore interesting to make comparisons with these spectra, since SDS is known to form well-ordered monolayers where the hydrocarbon chain protrudes out of the liquid with few CH_2 gauche (skewed) defects. The CH_3-FR (at 2935 cm^{-1}) is the dominant peak in the SDS BBSFG spectrum, the CH_3-SS is much smaller (2872 cm^{-1}), and the CH_2-SS

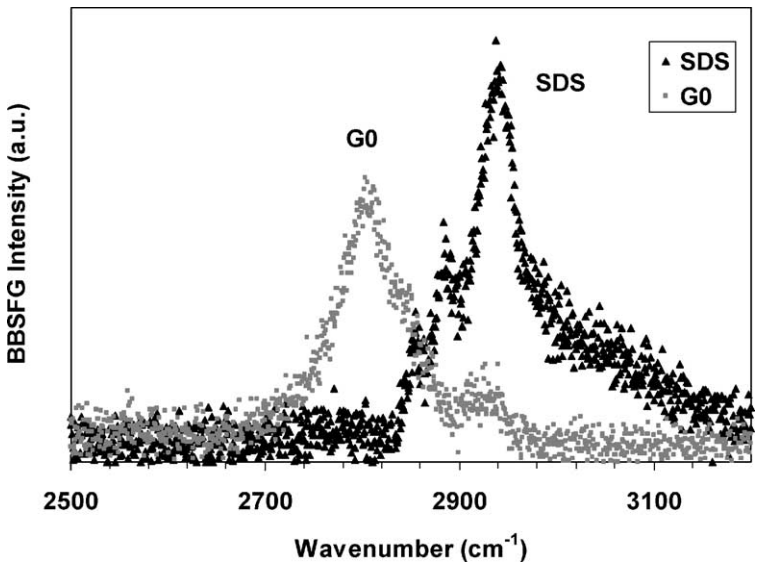

Fig. 5. BBSFG spectrum (SSP polarization) of a monolayer of sodium dodecyl sulfate (taken from a 1 mM SDS aqueous solution) and a BBSFG spectrum of PAMAM G1 gel using a 2 min acquisition time.

(2844 cm^{-1}) is small relative to the other peaks (the CH_2-AS is not observed in the SDS spectrum). The intensity of the CH_3-FR and SS dominate since the SSP polarization combination couples efficiently with the transition moments that are normal to the surface, in this case, the CH_3-SS. Yet the CH_2-SS only has a small contribution to the SFG intensity from the SDS since the SS of the methylene groups on the hydrocarbon chain are in the plane of the surface and local symmetry cancels their SFG intensities. Therefore, because of local symmetry (the CH_2 groups oppose each other—dominantly *trans*-) and because of the lateral direction of the CH_2-SS transition moment, the SFG response is minimal. The small peak that is observed has been attributed to the small number of CH_2 gauche defects in the SDS hydrocarbon chains [29,35]. In addition, there is an odd number of CH_2 groups (11 CH_2 groups) on the SDS hydrocarbon chain, and therefore, even in the instance of a completely *trans*-hydrocarbon chain, one might expect to observe a CH_2 contribution from the odd CH_2. For the PAMAM G0 spectrum shown for comparison with the SDS SFG spectrum in Fig. 5, the CH_2-SS peak is substantially larger than that from SDS and is clearly broad. One can deduce that the peak broadness is due to the differing chemical environments within the PAMAM G0 dendrimer. The substantial peak intensity implies that there is a lack of *trans*-methylene configurations and yet there is a net ordering of the CH_2 groups taking place within the perpendicular plane at the surface of the dendrimer gel. This is also confirmed by the fact that the CH_2-AS from the PAMAM G0 is relatively small and that the spectrum is dominated by the CH_2-SS. Ordering refers to the net orientation of the CH_2 groups relative to one another. A purely *trans*-configuration would cancel the SFG response. For example: If one CH_2 of the PAMAM pointed out from the surface and another chemically equivalent CH_2 of the PAMAM pointed toward the bulk gel, we would expect cancellation of the SFG response, somewhat similar to that observed for the CH_2-SS in the SDS SFG spectrum of Fig. 5. Any gauche or skewed defects would give rise to a net SFG response from the CH_2-SS modes. Upon examination of the PAMAM G0, G1, and AcPAMAM G0 (Fig. 1a–c), the methylenes occur in groups of two throughout the dendrimer structures. This provides local inversion symmetry only if the two CH_2 groups are exactly *trans*-relative to one another; however, we observe a significant SFG response. This suggests the non-*trans* configurations of the adjacent CH_2 groups. Additionally, since the CH_2-SS is substantially larger than the CH_2-AS, we also conclude that the orientations of the CH_2 groups are generally distributed

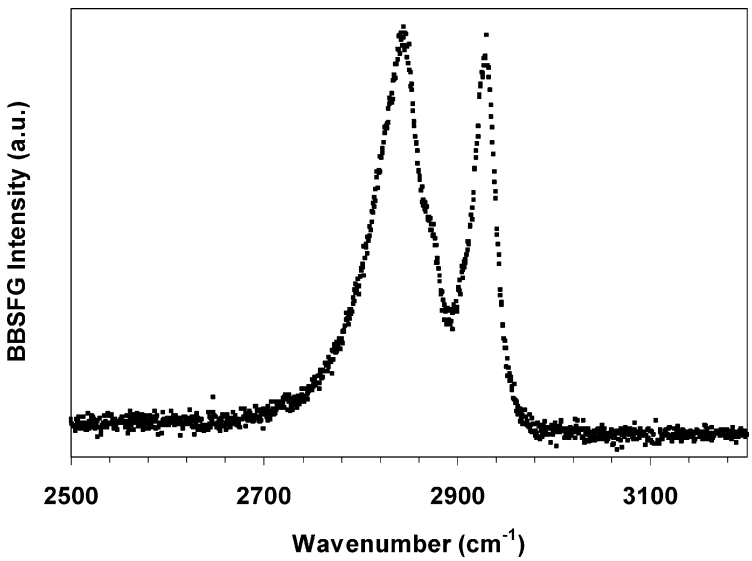

Fig. 6. BBSFG spectrum (SSP) of Ac-G0 after deposition on a glass slide using a 5 min acquisition time.

perpendicular to the surface plane. Additional polarization SFG studies are needed to infer the breadth of the distribution about the surface normal. These findings also suggest that the dendritic arms of the PAMAM G0 and G1 extend out in a somewhat planar arrangement, which is consistent with AFM [19–24] and contact angle measurements [21,26].

The SFG intensity shown in Fig. 4a and b, and the PAMAM spectrum in Fig. 5 is dominated by the SFG response from the air–dendrimer interface. The reflected visible and infrared beams that interact to produce the SFG intensity can penetrate the dendrimer gel and, in addition to probing the air–dendrimer interface, can also effectively probe the dendrimer–glass interface. However, in the case of the PAMAM G0 and G1, we estimate the thickness of the gel to encompass multiple layers. SFG contribution from the glass surface is not observed.

The acylated PAMAM G0 (Ac-G0) at the surface of a glass slide was also studied and the BBSFG spectrum is shown in Fig. 6. Two BBSFG peaks are observed, 2843 and 2930 cm^{-1}, and are attributed to the CH_2-SS modes and CH_3-FR modes, respectively. The shoulder at 2872 cm^{-1} is attributed to the CH_3-SS. One of the major differences between the SFG spectra of G0 and Ac-G0 is that the CH_2-SS peak position has changed. Since SFG responses can interfere constructively or destructively with one another based on their relative phases, the peak position change is not necessarily significant. These results are preliminary, and fitting the peaks with phase information will help to shed light on the true peak positions. However, it is clear that the CH_3-FR is of significant relative intensity along with the CH_3-SS shoulder on the adjacent peak, and this strongly suggests an ordering of the CH_3 end groups of the dendritic arms. For the Ac-G0, each dendrimer contributes 4 CH_3 groups and 18 CH_2 groups. Since the SFG response arises from a convolution of surface number density and orientation, for similar transition moment strengths, we can infer that a strong SFG response of a low-density moiety suggests a net orientation of this group (i.e. the CH_3 end groups) relative to the higher density moieties (the CH_2 groups). This is not necessarily surprising, given the fact that the CH_3 end groups can easily rotate. However, it is not clear if the CH_3 groups are pointing toward the bulk or toward the air. In addition, the Ac-G0 film on the glass slide is significantly thinner than that used in the G0 and G1 BBSFG studies, and it is not clear if the SFG signal intensity is dominated by the air–dendrimer surface. Studies are planned to differentiate the dominant source of the SFG. This is also true for the PAMAM G0 dendrimer film on the gold surface. This BBSFG spectrum is shown in Fig. 7. The peaks from the CH_2

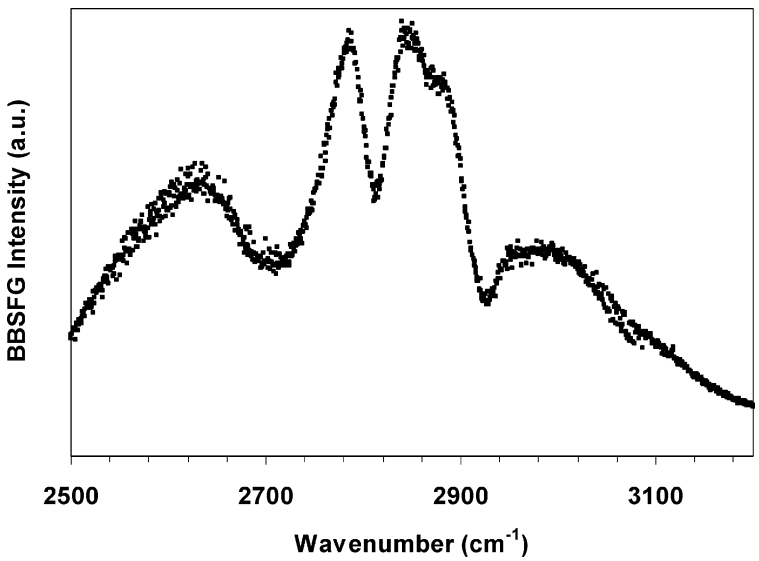

Fig. 7. BBSFG spectrum (SSP) of G0 after deposition on a bare gold surface using a 2 min acquisition time.

stretching modes are observed as dips in the spectrum. The peaks (dips) at 2802 and at 2943 cm^{-1} are assigned to the CH_2-SS and the CH_2-AS, respectively and are consistent with the assignments from PAMAM G0 on the glass slide (Fig. 3) as discussed above. The PAMAM G0 CH_2 peaks are inverted showing that there is a phase mismatch with the nonresonant SFG response from the gold and the resonant response from the dendrimer [36,37]. Although the PAMAM G0 dendrimer gel is multilayered on the gold surface (more so than the Ac-G0 on the glass slide), the enhanced reflectivity and recombination of the SFG response from both the air–dendrimer surface and the dendrimer–gold surface will complicate the phase interpretation of this spectrum. This complexity can be deconvoluted upon knowledge of the exact film thickness. These studies are also planned for the future.

4. Conclusions

Amine-terminated Starburst® PAMAM G0, G1 and acylated PAMAM G0 dendrimers have been studied using surface vibrational broadband sum frequency generation spectroscopy and Raman spectroscopy. Using BBSFG spectroscopy, it was revealed that methylene groups of the PAMAM G0 and G1 dendrimers on the surface of the deposited dendrimer gel were orientationally ordered. For each group of two methylenes, a non-*trans* orientation relative to each other is inferred. This conformation distribution is consistent with the dendron arms extending out from the central ethylenediamine core with the CH_2 groups distributed about the surface normal in a somewhat skewed configuration. Additional BBSFG and Raman studies are planned to further elucidate the structural conformations of the PAMAM G0, G1, Ac-G0, and higher generation PAMAM dendrimers at various interfaces.

Acknowledgements

The authors thank Professor Jon Parquette for his invaluable assistance throughout the synthetic modification portion of this work. We also acknowledge the US Coast Guard for funding support through the US Coast Guard Advanced Education Program. In addition, we thank InPhotonics Inc. and Process Instruments Inc. for the loan of the 785 nm Raman probe and the 785 nm diode laser.

References

[1] J.M.J. Fréchet, D.A. Tomalia, Dendrimers and Other dendritic polymers, Wiley, Chichester, New York, 2001.
[2] D.A. Tomalia, Sci. Am. 272 (1995) 62.
[3] R.F. Service, Science 267 (1995) 458.
[4] Y. Sayed-Sweet, D.M. Hedstrand, R. Spinder, D.A. Tomalia, J. Mater. Chem. 7 (1997) 1199.
[5] R. Esfand, D.A. Tomalia, DDT 6 (2001) 427.
[6] P.R. Dvornic, A.M.D. Leuze-Jallouli, M.J. Owen, S.V. Perz, Macromolecules 33 (2000) 5366.
[7] B. Huang, J.R. Parquette, Org. Lett. 2 (2000) 239.
[8] A.W. Bosman, H.M. Janssen, E.W. Meijer, Chem. Rev. 99 (1999) 1665.
[9] A. Topp, B.J. Bauer, D.A. Tomalia, E.J. Amis, Macromolecules 32 (1999) 7232.
[10] W. Chen, D.A. Tomalia, J.L. Thomas, Macromolecules 33 (2000) 9169.
[11] M.I. Ranasinghe, O.P. Varnavski, J. Pawlas, S.I. Hauck, J. Louie, J.F. Hartwig, T. Goodson III, J. Am. Chem. Soc. 124 (2002) 6520.
[12] C.L. Larson, S.A. Tucker, Appl. Spectrosc. 55 (2001) 679.
[13] D.A. Wade, P.A. Torres, S.A. Tucker, Anal. Chim. Acta 397 (1999) 17.
[14] M. Wells, R.M. Crooks, J. Am. Chem. Soc. 118 (1996) 3988.
[15] H. Nagaoka, T. Imae, Trans. Mater. Res. Soc. Jpn 26 (2001) 945.
[16] A. Manna, T. Imae, K. Aoi, M. Okada, T. Yogo, Chem. Mater. 13 (2001) 1674.
[17] R.E.A. Dillon, D.F. Shriver, Chem. Mater. 13 (2001) 1369.
[18] G. Bar, S. Rubin, R.W. Cutts, T.N. Taylor, J. Thomas, A. Zawodzinski, Langmuir 12 (1996) 1172.
[19] A. Hierlemann, J.K. Campbell, L.A. Baker, R.M. Crooks, A.J. Ricco, J. Am. Chem. Soc. 120 (1998) 5323.
[20] W.M. Lackowski, J.K. Campbell, G. Edwards, V. Chechik, R.M. Crooks, Langmuir 15 (1999) 7632.
[21] T. Imae, M. Ito, K. Aoi, K. Tsutsumiuchi, H. Noda, M. Okada, Colloids Surf. A 175 (2000) 225.
[22] J. Li, L.T. Piehler, D. Qin, J.R. Baker, D.A. Tomalia, Langmuir 16 (2000) 5613.
[23] G. Sui, M. Micic, Q. Huo, R.M. Leblanc, Langmuir 16 (2000) 7847.
[24] T.A. Betley, M.M.B. Holl, B.G. Orr, D.R. Swanson, D.A. Tomalia, J.R. Baker, Langmuir 17 (2001) 2768.
[25] K.M.A. Rahman, C.J. Durning, N.J. Turro, D.A. Tomalia, Langmuir 16 (2000) 10154.
[26] H. Tokuhisa, M. Zhou, L.A. Baker, V.T. Phan, D.L. Dermody, M.E. Garcia, R.F. Peez, R.M. Crooks, T.M. Mayer, J. Am. Chem. Soc. 120 (1998) 4492.
[27] D.C. Tully, J.M.J. Fréchet, Chem. Commun. 2001 (2001) 1229.
[28] Y.R. Shen, The Principles of Nonlinear Optics, Wiley, New York, 1984.

[29] P.B. Miranda, Y.R. Shen, J. Phys. Chem. B 103 (1999) 3292.
[30] D.E. Gragson, G.L. Richmond, J. Phys. Chem. B 102 (1998) 3847.
[31] H.C. Allen, D.E. Gragson, G.L. Richmond, J. Phys. Chem. B 103 (1999) 660.
[32] H.E. Gottlieb, V. Kotlyar, A. Nudelman, J. Org. Chem. 62 (1997) 7512.
[33] E.L. Hommel, G. Ma, H.C. Allen, Anal. Sci. 17 (2001) 1325.
[34] V.I. Kovalenko, V.L. Furer, A.E. Vandyukov, R.R. Shagidullin, J.P. Majoral, A.-M. Caminade, J. Mol. Struct. 604 (2002) 45.
[35] D.E. Gragson, B.M. McCarty, G.L. Richmond, J. Am. Chem. Soc. 119 (1997) 6144.
[36] K.A. Briggman, J.C. Stephenson, W.E. Wallace, L.J. Richter, J. Phys. Chem. B 105 (2001) 2785.
[37] A.G. Lambert, D.J. Neivandt, A.M. Briggs, E.W. Usadi, P.B. Davies, J. Phys. Chem. B 106 (2002) 5461.

Heather C. Allen received her B.S. degree in Chemistry (1993) and Ph.D. in Physical Chemistry (1997) at the University of California, Irvine. Her undergraduate advisor was Professor F.S. Rowland (1995 Nobel Laureate), and her graduate advisor and co-advisor were Professors J.C. Hemminger and B.J. Finlayson-Pitts, respectively. She was funded through several fellowships, Fannie and John Hertz, EPA, and NSF Traineeship fellowships. Dr. Allen worked as a NOAA Post-Doctoral Fellow in Climate and Global Change. This prestigious fellowship was awarded for her proposal based upon the use of nonlinear spectroscopy to be conducted in the G.L. Richmond Lab to study surfaces relevant to aerosol chemistry. While at The Ohio State University as an Assistant Professor of Chemistry, Dr. Allen was awarded the research Innovation Award from Research Corp. in 2001, an OSU-OMA Distinguished Professional Mentor Award in 2001, and an NSF CAREER Award in 2002.